

ZTF J185259.31+124955.2: A new evolved disc-eclipsing binary system

Klaus Bernhard¹ and Christopher Lloyd²

¹ Bundesdeutsche Arbeitsgemeinschaft für Veränderliche Sterne e.V. (BAV), Munsterdamm 90, D-12169 Berlin e-mail: klaus.bernhard@liwest.at

² Department of Physics and Astronomy, University of Sussex, Brighton, BN1 9QH e-mail: C.Lloyd@sussex.ac.uk

Received 1 April 2024 / Accepted 20 May 2024

ABSTRACT

Discs in long-period eclipsing binary systems are rare and can lead to extraordinary eclipsing events. ZTF J185259.31+124955.2 was identified as a candidate disc-eclipsing system through a continuing search programme of ZTF variables with a near-IR excess in the WISE data. Examination of the combined ZTF and ATLAS photometry shows seven eclipses since 2017 with depths of $0^m.34$ in all bands on a period of 289.57 ± 0.09 d. The eclipse width is ~ 40 d but this and the profile evolve over time. Comparison with library spectra shows that the spectral energy distribution from the available photometry is consistent with an early K-type giant, and fitting black-body profiles suggests $T_{\text{eff}} \sim 4000$ K for the stellar component, with a cool component having $T_{\text{eff}} < 500$ K. The reddening and distance, and hence the luminosity place the star within the giant branch. The most likely scenario is that the system is in a state of rapid evolution following Case B/C mass transfer into an extended disc around an unseen companion.

Key words. Stars: AGB and post-AGB – Stars: binaries: eclipsing – Stars: individual: ZTF J185259.31+124955.2 – Stars: evolution

1. Introduction

Although very rare, there are several long-period eclipsing binaries that show evidence of large, thin equatorial dust discs. These systems are unusual and complex variables, and frequently show changes in behaviour over time. They are an inhomogeneous group, but divide very broadly into pre-main-sequence and evolved systems. The most well-known eclipsing-disc system is the 27.1-year binary ϵ Aurigae, in which the brighter component, apparently an F-type giant, is eclipsed by an accretion disc surrounding an unseen, more massive companion, most likely a B-type star. The system is probably the result of late Case B or Case C mass transfer (see Gibson & Stencel 2018). The other well-known system is EE Cephei, which has a period of 5.6 years and consists of a Be-star and a dark dusty disc around an unseen companion (see Gałan et al. 2012; Pieńkowski et al. 2020). More recently the OGLE variable, OGLE-LMC-ECL-11893 (OGLE J05172127–6900558) has also been identified as another evolved system containing a B9 IIIe star, which undergoes a complex two-stage, asymmetric eclipse every 468 days, by an extended disc, with a compact core (see Dong et al. 2014; Scott et al. 2014).

Periodic variations due to dust are also seen in pre-main-sequence stars, but differences in geometry and the distribution of dust leads to a disparate mix of single, binary and triple systems. Both V1400 Cen (= J1407, $P \sim 5.4$ yr ? Mamajek et al. 2012; Barentloo et al. 2021) and V928 Tau ($P > 66$ d, van Dam et al. 2020) show deep eclipse-like features, but without any clear periodicity. The unusual pre-MS stars V718 Per ($P = 4.7$ yr Grinin et al. 2008) and CHS 7797 (= V2187 Ori, Rodríguez-Ledesma et al. 2012, 2013) both have amplitudes of $\Delta I \sim 0^m.7$ and approximately sinusoidal variations, but the periods are very different at 4.7 yr and 17.8 d respectively, and V718 Per is probably a single star, while the nature of CHS 7797 is still unclear. In

contrast, the light curves of the low-amplitude Orion-type variables VSSG 26 (= WL 4, $P = 131$ d, Plavchan et al. 2008) and YLW 16A ($P = 93$ d, Plavchan et al. 2013) are more nearly square waves.

VSSG 26, YLW 16A and CHS 7797 are often compared to Kearns-Herbst 15D (KH 15D = V582 Mon, Kearns & Herbst 1998), which now constitutes the prototype of category of circumbinary disc systems. Photometric and spectroscopic observations have shown that the circumbinary disc is tilted relative to the central, highly eccentric binary. In a previous study Zhu et al. (2022) reported a search for additional KH 15D objects, and identified two further candidates, ZTF J202055.22+381323.1 ('Bernhard 1') and ZTF J071445.39–090152.1 ('Bernhard 2'). A characteristic of KH 15D, as well as the two other identified candidates, is a large amplitude exceeding 2 magnitudes in the I-band at the time of their discovery. However, long-term time series analysis of KH 15D, such as the study by Poon et al. (2021) reveals that these objects do not consistently display such high amplitude variations. The aim of this new study was to search for additional disc-related long-period eclipsing binary systems in the ZTF database, focusing on lower amplitude variations.

2. Observations

The starting point of this search is the ZTF catalogue of variable stars by Chen et al. (2020), which contains about 780,000 periodic variables with provisional classifications. The catalogue is based on data from the Zwicky Transient Facility (ZTF), which is a time-domain survey using the 48-inch Palomar Schmidt Telescope and has been in operation since 2017. Observations are made in the three different Sloan passbands g (414–546 nm), r (566–721 nm) and partly i (721–873 nm) on a cadence of 1–2 d, and to a limiting magnitude of 20.5. ZTF data are therefore

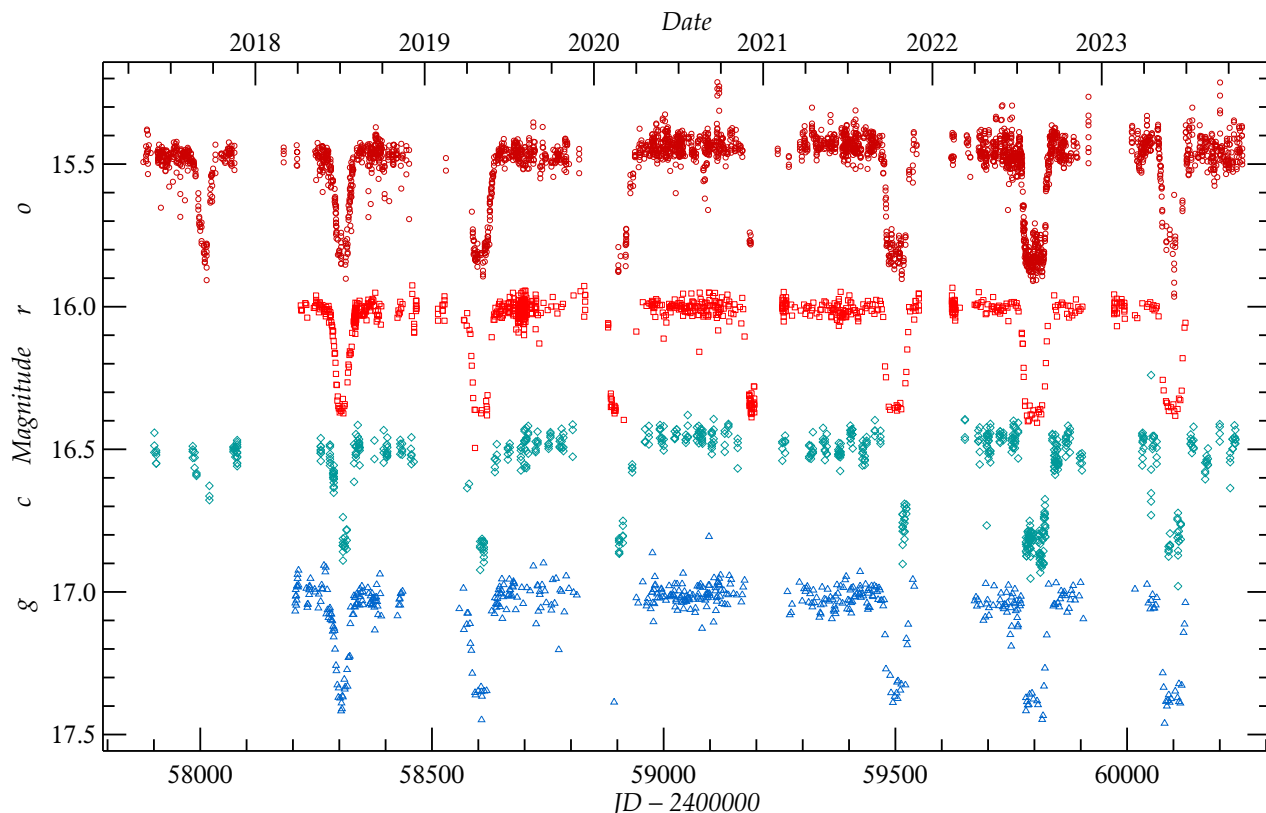


Fig. 1. Light curve from ATLAS and ZTF showing the bands with different symbols. These are in order of decreasing effective wavelength, from o (top) through r and c to g (bottom), with small offsets to aid visibility ($r + 0.3$, $c - 0.1$, $g - 0.5$).

ideally suited for studies of variable stars (Bellm et al. 2019; Masci et al. 2019). Supplementary data were acquired through the ‘cyan’ c band (420–650 nm), and the ‘orange’ o band (560–820 nm) of the ATLAS Forced Photometry web service (Tonry et al. 2018; Heinze et al. 2018; Shingles et al. 2021). The initial study (Zhu et al. 2022) focused on identifying eclipsing variable objects with periods greater than 10 days and amplitudes exceeding 1.5 magnitudes in the two ZTF catalogues of variable stars, which included also a list of approximately 1,000,000 suspected variables. By contrast, this research is centred on investigating smaller amplitude variations, specifically in the range of about 0.5 to 1.5 magnitudes. Due to the selection of smaller amplitudes, a substantially larger pool of candidates emerged (19 649 compared to 1 041). As an additional selection, only those objects displaying clear indications of a cool disc in the WISE colours (Cutri et al. 2021) were examined in detail. This process yielded 19 objects, which were then subjected to visual inspection.

3. Results

Examination of the light curves of the 19 candidates suggests that the majority are, superficially, eclipsing binary systems without any particularly distinguishing features. However, one shows an evolving eclipse, characteristic of a disc system, which is the subject of this paper, while two others show different unusual features and will be reported elsewhere (Bernhard & Lloyd, in prep.). The most promising candidate, ZTF J185259.31+124955.2, is categorized as an EA-type variable with a 290-day period by Chen et al. (2020). ZTF J185259.31+124955.2 is recorded as *Gaia* DR3

4506139331756845568 (18 52 59.315 +12 49 55.287, J2000), with an average brightness of $G = 15.63$ from the *Gaia* DR3 data as listed in VizieR. The *Gaia* Apsis processing gives a distance of 2900 pc leading to an absolute magnitude of $M_G = 1.4$, and its effective temperature $T_{\text{eff}} = 4831$ K suggests that the star is a giant (Gaia Collaboration et al. 2023; Gaia Collaboration 2022).

The light curve from 2017 is shown in Fig. 1 for the ATLAS o and c bands, and the ZTF g and r bands. A significant number of ZTF i -band observations were made during 2020, but these miss the eclipses and provide only the out-of-eclipse magnitude in this band, so are not shown here. A small number of ATLAS observations are also available from 2015 and 2016, but these are sparse and again miss the eclipses, so they are not shown here, although they are included in the analysis later. The different bands are shown close to their natural magnitudes, but with small offsets to aid visibility ($r + 0.3$, $c - 0.1$, $g - 0.5$), and this means that the bands appear in order of decreasing effective wavelength, from o , through r and c to g . The ATLAS bands are both very broad, ~ 220 nm, and their short-wavelength limits are essentially coincident with those of the ZTF g and r bands, but these are narrower, so they effectively cover approximately the shorter-wavelength half of the c and o bands. It should also be pointed out that the out-of-eclipse magnitude in the ATLAS photometry is not completely constant, and shows a small brightening through the data of perhaps $0^m.05$, and other small coherent excursions, that are not seen in the ZTF data.

The light curve itself shows evidence of eight eclipses, with a period close to 290 d, as suggested by Chen et al., and this is supported by a high-order Fourier fit, which confirms that the variation is periodic. However, even at this point it is clear that

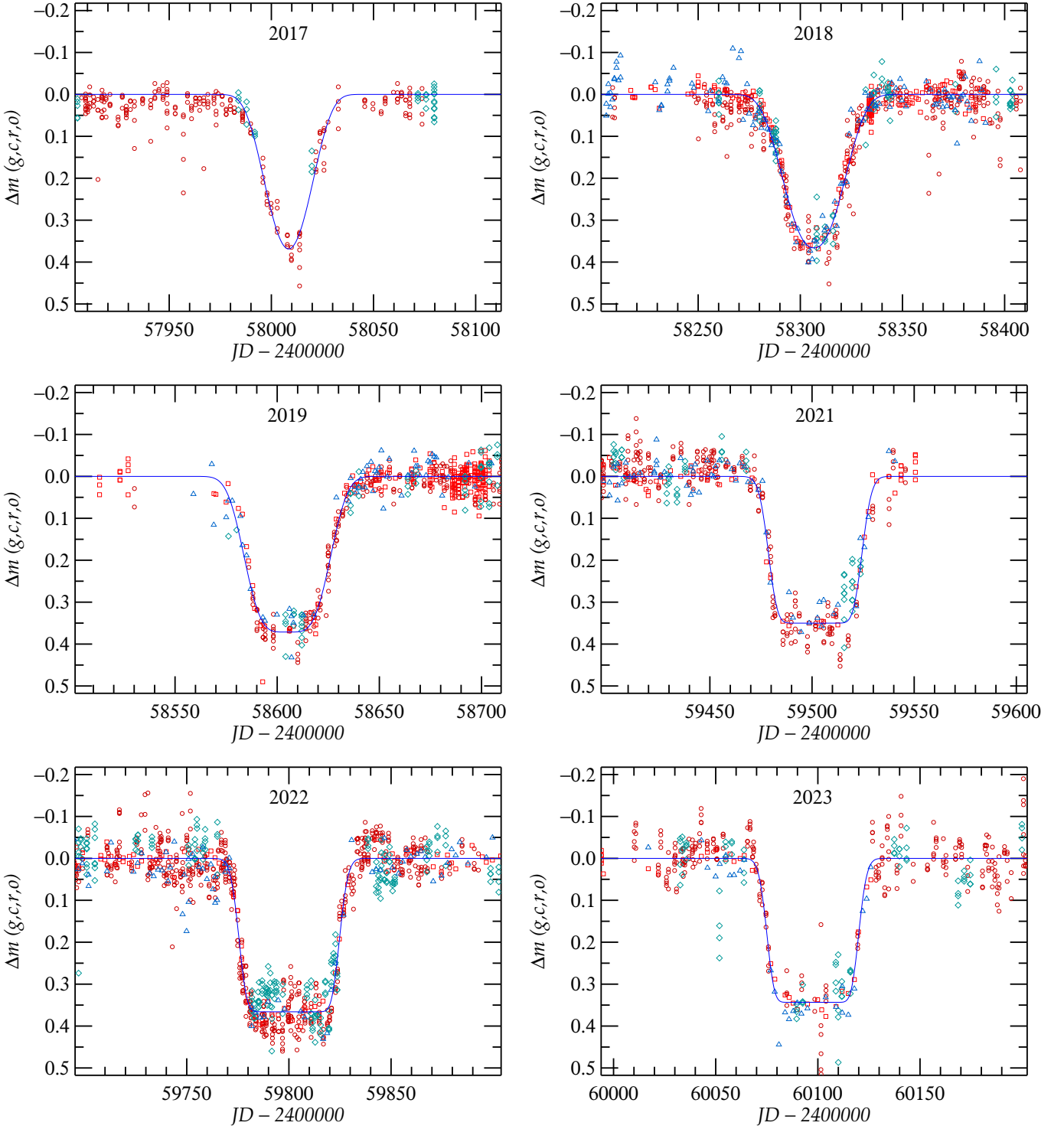


Fig. 2. Evolution of the shape and width of the eclipse using the magnitude offsets for all the bands as available, relative to the out-of-eclipse values. The symbols are as before.

the later eclipses are broader than the earlier ones, and also that the eclipse depth is constant across all four bands at approximately $0^m.4$.

In an effort to quantify the properties of the light curves they have been modelled using the methodology described by Mikulášek (2015), which can fit a wide variety light curve shapes, from exo-planet and simple detached, partial and total EBs to complex W UMa types, using a small number of param-

eters. It is not a physical representation, but a mathematical parameterization of the light curve. The expression used is their Equation 13 in the single, primary eclipse form. After some experimentation it was decided to eliminate the effect of the 'curvature' coefficient, C_k , by setting this to zero. On the present data sets this term allowed too much flexibility and produced unnatural and unjustified features in the fits. The parameters that can be determined directly from the fits are the central time, the zero

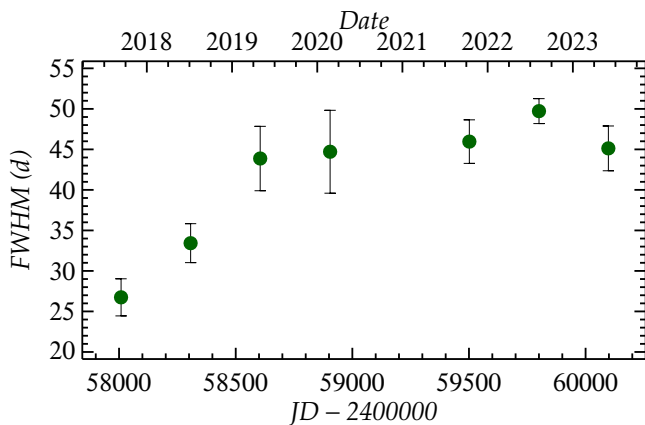


Fig. 3. Full width at half minimum of the observed minima from the combined data as given in Table 1.

Table 1. Parameters of fits to combined minima

HJD	O-C (d)	E	Depth (mag)	FWHM (d)
2458008.20(40)	-0.1	0	0.375(11)	27.2±2.2
2458306.65(21)	-0.2	1	0.365(9)	33.4±2.4
2458605.05(32)	-0.4	2	0.370(7)	43.9±3.9
2458904.70(50)	0.7	3	0.352(9)	44.7±5.0
2459501.47(22)	0.3	5	0.350(6)	46.4±2.7
2459800.16(13)	0.4	6	0.365(3)	49.7±1.5
2460097.51(25)	-0.8	7	0.343(6)	45.1±2.8

level, that is the out-of-eclipse magnitude, and the depth of the minimum. Less directly, it is also possible to measure the full width half maximum (FWHM) of the eclipse profile. Preliminary fits to the individual minima in the different bands immediately revealed that the depths of the eclipses are very similar in all bands, and over time. Using this it was possible to improve the statistics, and coverage, of the individual minima by combining the data from different bands. The two eclipses from 2020 are poorly covered, and the later one is only observed on the ingress, so parameters were derived for seven of the eclipses. The six best-observed minima and their fits are shown in Fig. 2. It is clear that over the period of observations the width of the eclipse has increased, and the shape of the profile has become apparently 'total'. The relevant parameters of the fits are listed in Table 1.

Examination of the individual minima shows that there is no consistent difference in the depth, or profile in the different bands. The largest difference is probably during the 2021 eclipse where it reaches perhaps 0^m05 between the blue and the red, but the scatter is large and there are other instances of similar offsets, in both directions, in the out-of-eclipse data, so its significance is not clear. The rms variation of the eclipse depths over time is 0^m014 , and is generally compatible with the measured uncertainties, although the first three eclipses are the deepest, but again the significance, if any, is not clear.

However, the variation in the eclipse width is clearly established. It is obvious in the plots of the individual minima and is shown directly in Fig. 3. The width increased from 27 to 44 d in the first three cycles and then appears to have remained constant since then. However, the profile continued to evolve from 2019 to 2021 with ingress and egress becoming progressively steeper, but with little change in the FWHM. The change in width of the

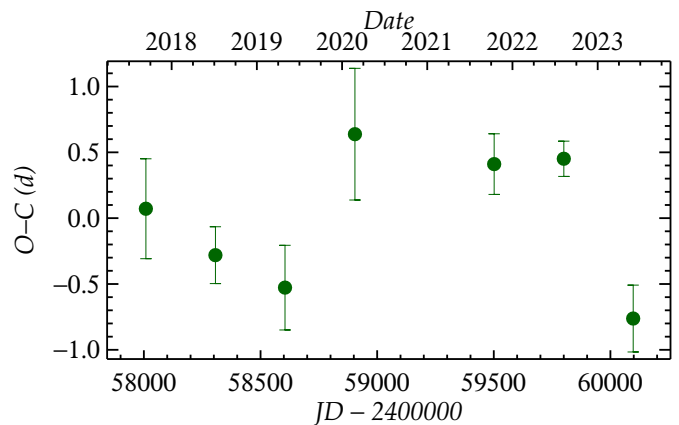


Fig. 4. O-C diagram constructed using the ephemeris in Equation 1 derived from the timings given in Table 1.

early eclipses is not matched by a change in gradient of the profile, and it appears that the eclipse simply broadened until 2019, when it becomes total.

Using the central time of the eclipse it is possible to derive a more reliable value for the period, and an unweighted linear fit gives an ephemeris of

$$HJD_{\text{Minl}} = 2458008.30 \pm 0.37 + 298.57 \pm 0.09 \times E \quad (1)$$

where the residuals are shown in the O-C diagram in Fig. 4. The rms residual of 0^d5 and the formal error on the period suggest that the period is very tightly constrained, despite the changes in the shape and width of the eclipse profile, and this suggests that the eclipse process is symmetric with respect to some dynamical clock in the system.

With an improved ephemeris it is possible to phase the individual bands and examine their mean light curves. These are shown in Fig. 5 with their individual fits. As the eclipse profile is known to change these fits provide only two useful parameters, the mean out-of-eclipse magnitude and the mean depth of the eclipse for each band. These values are collected in Table 2. However, the plot also demonstrates that the changes to the eclipses are symmetric and further supports the conclusions from the O-C diagram. Given the constancy of the ZTF *r*-band out-of-eclipse photometry, it is probably the most reliable, so the eclipse also has constant brightness during minimum light.

4. Spectral energy distribution and luminosity

As mentioned earlier the star is most likely a cool giant, and was also selected on the basis of an excess in the WISE infrared flux. The full spectral energy distribution (SED) has been explored using mean magnitude measurements covering a wide wavelength range from *Gaia* DR3 *G*, *G_{BP}*, *G_{RP}*, ZTF *gri*, Pan-STARRS *grizy* (Chambers et al. 2016), 2MASS *JHK_s* (Cutri et al. 2003; Skrutskie et al. 2006) and WISE *W1*, *W2*, *W3*, and *W4* (Wright et al. 2010; Cutri et al. 2021). These have compared to a range of spectra from the Pickles (1998) Stellar Flux Library using a minimization scheme that can treat the reddening as a free parameter. The photometry was compared with the luminosity class III library spectra of F5, G0, G5, K0, K5, M0 and M3 stars, out to 2 microns. The best fit was achieved for each of the library spectra with reddening E_{B-V} of 1.27, 1.06, 0.96, 0.89, 0.44, 0.32, and 0.06 respectively. The best fits were achieved with the G0 III, G5 III, K0 III and K5 III spectra, which are all

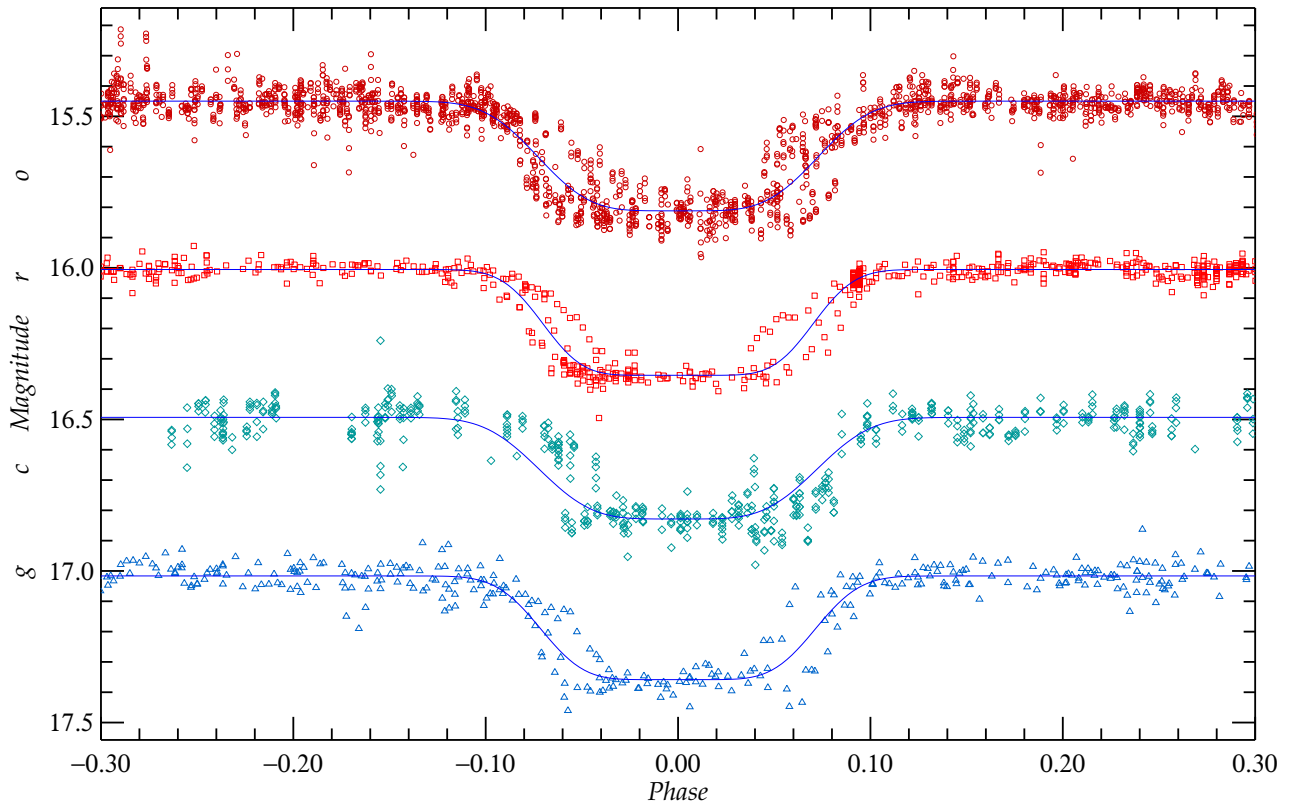


Fig. 5. Phased light curve of the ATLAS *o* and *c*-band and ZTF *r* and *g*-band data, based on the ephemeris Equation 1. The magnitude offsets and symbols are the same as Fig. 1.

Table 2. Mean photometric data

	ZTF <i>g</i>	ATLAS <i>c</i>	ZTF <i>r</i>	ATLAS <i>o</i>	ZTF <i>i</i>
Maximum	17.516(2)	16.595(2)	15.705(2)	15.450(1)	14.927(3)
Depth	0.342(8)	0.334(6)	0.349(7)	0.361(4)	–

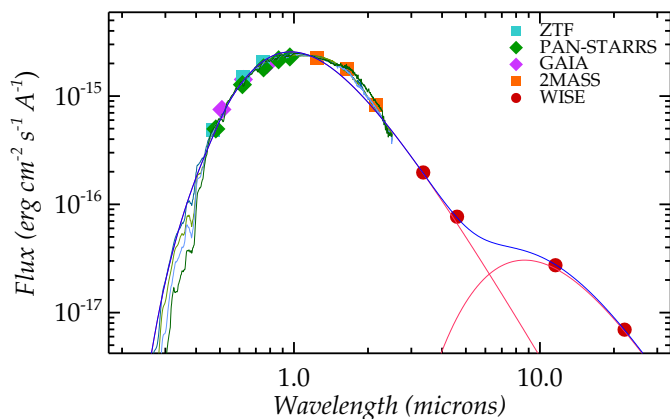


Fig. 6. Spectral energy distribution showing the observed fluxes with the optimally reddened G0 III, G5 III, K0 III and K5 III library spectra. The red lines are the individual black-body fits and the blue line is the combined two-component fit.

very similar and were significantly better than F5 III and the later spectral types. The observed SED and the optimally reddened fits for these spectra are shown in Fig. 6. While the WISE W1 and W2 photometry at 3.35 and 4.6 μm may be consistent with

these spectra the W3 and W4 bands beyond 10 μm are clearly incompatible and suggest an additional cool component. So, the data have been fitted with a two-component black-body, however, the solution is poorly constrained so some limitations have been imposed. Equal relative errors have been assumed on the photometry, and the reddening has been fixed, in the case illustrated at $E_{B-V} = 0.6$. The optimal black-body temperatures are $T_1 = 3940 \pm 280$ K and $T_2 = 340 \pm 140$ K, and with larger reddening, higher temperatures result, with a sensible limit of $T_1 \sim 4500$ K, and it is difficult to force T_2 above 400–500 K. The *Gaia* Apsis processing chain gives $T_{\text{eff}} = 4830$ K.

The luminosity of the system is obviously dependent on the distance, and to some extent so is the reddening. However, there is no consensus on the distance. The parallax from *Gaia* is $\Pi = 0.153 \pm 0.039$ mas, which leads directly to a rather uncertain $d = 6500^{+2200}_{-1300}$ pc. [Bailer-Jones et al. \(2021\)](#) provide two *Gaia*-derived distances, one from geometric distance posterior (*rgeo*) of 5400^{+1700}_{-900} pc, and a second from the photogeometric distance posterior (*rpgео*) of 4740^{+925}_{-670} pc, which lead to a 1-sigma range of 4100–7100 pc. As mentioned earlier the *Gaia* Apsis processing gives a surprisingly low distance of 2609 pc, and well outside the range of the other estimates.

Based on the *Gaia* photometry Apsis gives the visual extinction as $A_V = 3.07$, which with $R_V = 3.1$ leads to $E_{B-V} = 0.99$. An independent measure of the reddening is provided by the 3D

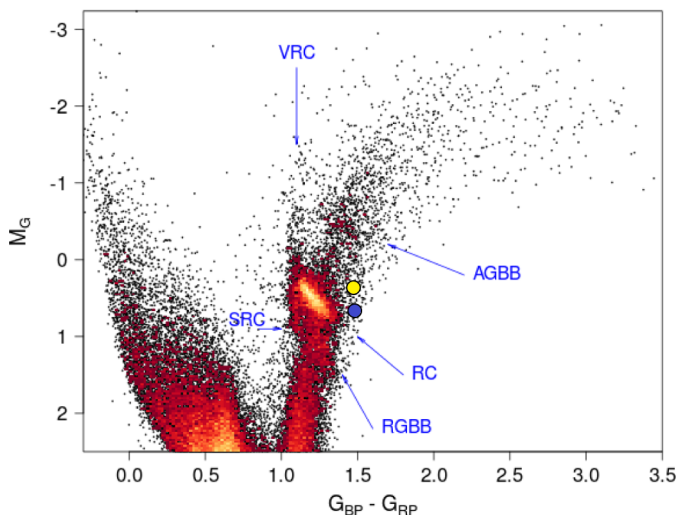


Fig. 7. Position of the star in the HR diagram. M_G is calculated using the minimum luminosity and assuming $E_{B-V} = 0.6$ for the *Gaia rgeo* (blue) and *rpgeo* (yellow) distances. The points are superimposed on the *Gaia* data for low-extinction nearby giants (Fig. 10 in [Gaia Collaboration et al. 2018](#)) and lie close to the Red Clump, and well within the distribution of a larger sample of stars (see e.g., Fig. 5 in the same paper).

Dust Maps of [Green et al. \(2019\)](#) who find $E_{g-r} = 0.60^{+0.08}_{-0.01}$ at 4740 pc, and that the reddening plateaus at $E_{g-r} = 0.69$ beyond 6000 pc. Unfortunately [Lallement et al. \(2018\)](#) do not provide any reddening estimates at this distance. From the available data, and assuming $E_{g-r} = E_{B-V}$ at this level of precision, then the system has $E_{B-V} > 0.6$, but probably < 1.0 , and this is broadly consistent with the findings from the SED. With the reddening in this range then $A_V \sim 2-3$ magnitudes, and using the [Wang & Chen \(2019\)](#) relationship, $A_G = 0.789A_V$, then the extinction in G , $A_G \sim 1.6-2.4$. With a mean magnitude out-of-eclipse of $G = 15.63$ then for the *rgeo* distance at 4740 pc $M_G = 0.7$ to -0.1 , while for the *rpgeo* distance at 5400 pc, $M_G = 0.4$ to -0.4 . The mean observed out-of-eclipse $G_{BP} - G_{RP} = 2.30$ so with $E_{B-V} = 0.6$ and using the relationship $E_{B-V} = 0.76E_{(G_{BP}-G_{RP})}$ then $(G_{BP}-G_{RP})_0 = 1.50$. The dereddened M_G and $(G_{BP}-G_{RP})_0$ magnitudes are plotted for both cases in the HR diagram in Fig. 7, and place the star well within the giant branch.

5. Discussion

As the object presents as a K-type giant, both in terms of luminosity and its SED, that immediately suggests that it is not a young or pre-main-sequence system, and must be evolved, like ϵ Aur or EE Cep, but on a very much smaller scale. It is most likely the result of late Case B or Case C mass transfer, where the K-type star has lost a high proportion of its mass and is now the secondary in a system, where the new primary is obscured by the accreted material, some of which is formed into an extended disc. From the SED it is clear that there is a faint, cool component in the system, and this is most likely emission from dust, which is also responsible for the grey eclipses. There is no indication of any other variation during the cycle, and nothing that could be interpreted as a secondary eclipse.

The eclipse is 0^m34 deep so this means that at minimum some 73% of the light in the system is uneclipsed. It is possible that the star is fully occulted, but that the optical depth is sufficiently low that a only a small fraction of light is scattered.

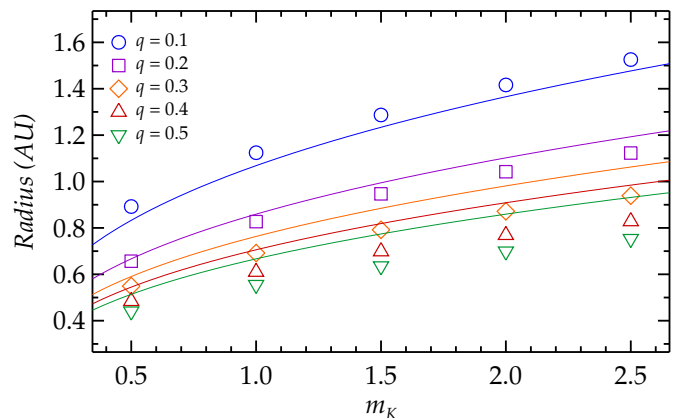


Fig. 8. Radius of the Roche lobe around the unseen component. The radius is calculated for sample mass ratios, q , as given by the symbols, for five possible masses of the K giant, assuming $r_K = 16 R_\odot$ (see text). The solid lines are the radii of an equatorial disc corresponding to the phase coverage of the eclipse, $\Delta\phi = 0.1$, colour-coded for the values of q . For $q = 0.1$ the equatorial disc lies within the Roche lobe, but for increasing values of q the radius of the eclipsing material progressively exceeds the Roche lobe by up to 22% at $q = 0.5$.

However, if the disc is relatively transparent then the other component should be visible, so this argues against a thin equatorial disc in the line of sight. If the disc has significant thickness, or is inclined to the orbital plane, then it is possible that the face of the K star is not completely covered, perhaps by a thin ring or other moving features in, or on the boundary of the disc. At present there is very little information to constrain the geometry of the system, but the eclipse variation demands some asymmetry, either as an inclined or thick disc. Another obvious question is what limits the duration of the eclipse, while simultaneously limiting its depth in a way that it appears to reach a saturation limit. One possibility is that eclipsed star contributes only 30% of the light to the system and is completely obscured by a variable disc, but that would require that the most visible component, the K giant, is not involved, and would effectively be a third light.

Assuming the least contrived arrangement of the components, that is with the lower-mass K-star secondary and a more massive dark primary component, with its circumstellar disc, then it is possible to draw some preliminary conclusions. Taking a range of K-star masses, $m_K = 0.5 \dots 2.5 M_\odot$ ([Hekker et al. 2011](#)), and mass ratios $q = m_K/m_{\text{dark}} = 0.1 \dots 0.5$, with the known period, it is possible to calculate the size of the system, which ranges from $a = 1.5$ to 2.6 AU for $q = 0.1$, to $a = 1.0$ to 1.7 AU for $q = 0.5$. Using the [Eggleton \(1983\)](#) approximation, it is possible to calculate the Roche lobe radii of both components for the various combinations of m_K and q . The results are shown in Fig. 8 where the symbols show the Roche lobe radii of the dark component. Assuming that the eclipse is due to an equatorial disc around the dark component then its radius can be calculated from the phase coverage of the eclipse, taken as $\Delta\phi = 0.1$, and these are shown as the solid lines. For $q = 0.1$ the radius of the eclipsing material lies just within the appropriate Roche lobe, but for the larger values of q the radius of the disc exceeds the Roche lobe by 5% at $q = 0.2$ and 22% at $q = 0.5$. If this scenario is physically meaningful then it suggests that the mass ratio $q > 0.2$. The radius of the K giant is not known, and given the likely history of the system may not be nominal for the spectral type, however, the luminosity and temperature are consistent with what is expected, so the radius probably is as well. Mean

radii of K giants are given as 16 ± 2 and $31 \pm 6 R_{\odot}$ at K1 III and K4 III respectively by Dyck et al. (1996), and more broadly red giants have a median radius of $10 R_{\odot}$, but these are dominated by red-clump stars (Hekker et al. 2011). The radius of the K giant also has a small impact on the calculation of the disc radius given above. There r_K was taken as $16 R_{\odot}$ but if the value of $31 R_{\odot}$ is used then the radius of the equatorial disc is reduced generally by $\sim 5\%$, and becomes entirely compatible with $q = 0.2$.

For the range of parameters used here the minimum Roche-lobe radius of the K giant is $68 R_{\odot}$ (0.32 AU) for $q = 0.1$ rising to $117 R_{\odot}$ (0.54 AU) for $q = 0.5$, largely irrespective of the total mass, so is significantly larger than the star in all cases. As the mass transfer has now ceased, the Roche lobe radius provides a fossilized record of the radius of the K giant at the time the system became detached. While all the possible radii are consistent with large giants or supergiants, the smallest radius for $q = 0.1$ represents the lowest fractional change, and may offer additional weak support for that value.

6. Conclusions

ZTF J185259.31+124955.2 is shown to be an unusual long-period eclipsing binary with precise periodicity (Equation 1), however the eclipse width and profile have changed symmetrically during the observations over the past seven years. The depth of the eclipse appears to have remained constant over time (see Fig. 2 and Table 1), and with wavelength (see Fig. 5 and Table 2), so the eclipse is grey, meaning that the occulting material is optically thin dust. The optical-NIR SED is consistent with an early K-type giant and with the observed reddening $E_{B-V} \approx 0.6$, and also shows a cool component consistent with extended dust. Any model of the system will need to explain the apparent limit or saturation of both the eclipse depth, which appears to be constant despite the other changes, and in width, where the eclipse widens and then apparently steepens. These changes appear to require some evolution or asymmetry in the disc. Assuming the most obvious scenario, the width of the eclipse is consistent with a disc lying within the Roche radius of the dark component for $q < 0.2$, as demonstrated in Fig. 8. The most obvious requirement for new observations is a spectroscopic study of the system, to further understand what is being eclipsed, and for radial velocities to place some constraints on the masses involved.

Acknowledgements. This paper made use of data from VizieR catalog access tool, of the interactive sky atlas Aladin, CDS, Strasbourg, France, the NASA/IPAC Infrared Science Archive and of the International Variable Star Index (VSX) database of the American Association of Variable Star Observers (AAVSO, Cambridge, Massachusetts, USA). It also utilizes data from the Asteroid Terrestrial-impact Last Alert System (ATLAS) project. This work has also made use of data from the European Space Agency (ESA) mission *Gaia* (<https://www.cosmos.esa.int/gaia>).

References

Bailer-Jones, C. A. L., Rybizki, J., Founesneau, M., Demleitner, M., & Andrae, R. 2021, *AJ*, 161, 147
 Barentloo, S., Dik, C., Kenworthy, M. A., et al. 2021, *A&A*, 652, A117
 Bellm, E. C., Kulkarni, S. R., Barlow, T., et al. 2019, *PASP*, 131, 068003
 Chambers, K. C., Magnier, E. A., Metcalfe, N., et al. 2016, arXiv e-prints, arXiv:1612.05560
 Chen, X., Wang, S., Deng, L., et al. 2020, *ApJS*, 249, 18
 Cutri, R. M., Skrutskie, M. F., van Dyk, S., et al. 2003, *VizieR Online Data Catalog*, II/246
 Cutri, R. M., Wright, E. L., Conrow, T., et al. 2021, *VizieR Online Data Catalog*, II/328
 Dong, S., Katz, B., Prieto, J. L., et al. 2014, *ApJ*, 788, 41
 Dyck, H. M., Benson, J. A., van Belle, G. T., & Ridgway, S. T. 1996, *AJ*, 111, 1705

Eggleton, P. P. 1983, *ApJ*, 268, 368
 Gaia Collaboration. 2022, *VizieR Online Data Catalog*, I/355
 Gaia Collaboration, Babusiaux, C., van Leeuwen, F., et al. 2018, *A&A*, 616, A10
 Gaia Collaboration, Vallenari, A., Brown, A. G. A., et al. 2023, *A&A*, 674, A1
 Gałan, C., Mikołajewski, M., Tomov, T., et al. 2012, *A&A*, 544, A53
 Gibson, J. L. & Stencel, R. E. 2018, *MNRAS*, 476, 5026
 Green, G. M., Schlafly, E., Zucker, C., Speagle, J. S., & Finkbeiner, D. 2019, *ApJ*, 887, 93
 Grinin, V., Stempels, H. C., Gahm, G. F., et al. 2008, *A&A*, 489, 1233
 Heinze, A. N., Tonry, J. L., Denneau, L., et al. 2018, *AJ*, 156, 241
 Hekker, S., Gilliland, R. L., Elsworth, Y., et al. 2011, *MNRAS*, 414, 2594
 Kearns, K. E. & Herbst, W. 1998, *AJ*, 116, 261
 Lallement, R., Capitanio, L., Ruiz-Dern, L., et al. 2018, *A&A*, 616, A132
 Mamajek, E. E., Quillen, A. C., Pecaut, M. J., et al. 2012, *AJ*, 143, 72
 Masci, F. J., Laher, R. R., Rusholme, B., et al. 2019, *PASP*, 131, 018003
 Mikulášek, Z. 2015, *A&A*, 584, A8
 Pickles, A. J. 1998, *PASP*, 110, 863
 Piefkowski, D., Gałan, C., Tomov, T., et al. 2020, *A&A*, 639, A23
 Plavchan, P., Gee, A. H., Stapelfeldt, K., & Becker, A. 2008, *ApJ*, 684, L37
 Plavchan, P., Güth, T., Laohakunakorn, N., & Parks, J. R. 2013, *A&A*, 554, A110
 Poon, M., Zanazzi, J. J., & Zhu, W. 2021, *MNRAS*, 503, 1599
 Rodríguez-Ledesma, M. V., Mundt, R., Ibrahimov, M., et al. 2012, *A&A*, 544, A112
 Rodríguez-Ledesma, M. V., Mundt, R., Pintado, O., et al. 2013, *A&A*, 551, A44
 Scott, E. L., Mamajek, E. E., Pecaut, M. J., et al. 2014, *ApJ*, 797, 6
 Shingles, L., Smith, K. W., Young, D. R., et al. 2021, *Transient Name Server AstroNote*, 7, 1
 Skrutskie, M. F., Cutri, R. M., Stiening, R., et al. 2006, *AJ*, 131, 1163
 Tonry, J. L., Denneau, L., Heinze, A. N., et al. 2018, *PASP*, 130, 064505
 van Dam, D. M., Kenworthy, M. A., David, T. J., et al. 2020, *AJ*, 160, 285
 Wang, S. & Chen, X. 2019, *ApJ*, 877, 116
 Wright, E. L., Eisenhardt, P. R. M., Mainzer, A. K., et al. 2010, *AJ*, 140, 1868
 Zhu, W., Bernhard, K., Dai, F., et al. 2022, *ApJ*, 933, L21

List of Objects

‘*ε Aurigae*’ on page 1
 ‘*EE Cephei*’ on page 1
 ‘*OGLE-LMC-ECL-11893*’ on page 1
 ‘*V1400 Cen*’ on page 1
 ‘*V928 Tau*’ on page 1
 ‘*V718 Per*’ on page 1
 ‘*V2187 Ori*’ on page 1
 ‘*VSSG 26*’ on page 1
 ‘*YLW 16A*’ on page 1
 ‘*KH 15D*’ on page 1
 ‘*ZTF J202055.22+381323.1*’ on page 1
 ‘*ZTF J071445.39–090152.1*’ on page 1